ISSN 0036-0236, Russian Journal of Inorganic Chemistry, 2021, Vol. 66, No. 1, pp. 117–123. © Pleiades Publishing, Ltd., 2021.
Russian Text © The Author(s), 2021, published in Zhurnal Neorganicheskoi Khimii, 2021, Vol. 66, No. 1, pp. 107–114.

INORGANIC MATERIALS AND NANOMATERIALS

Nanocrystalline TiO_2 Films: Synthesis and Low-Temperature Luminescent and Photovoltaic Properties

T. M. Serikov[a, *], N. Kh. Ibrayev[a], O. Ya. Isaikina[b], and S. V. Savilov[b, c]

[a] *Buketov Karaganda University, Karaganda, 100028 Kazakhstan*
[b] *Moscow State University, Moscow, 119991 Russia*
[c] *Kurnakov Institute of General and Inorganic Chemistry, Russian Academy of Sciences, Moscow, 119991 Russia*
**e-mail: serikov-timur@mail.ru*

Received June 15, 2020; revised August 5, 2020; accepted August 15, 2020

Abstract—Nanocrystalline TiO_2 films of different morphology have been fabricated using various experimental approaches. Photoluminescent properties of films at 90 K have been studied. The effect of heat treatment on low-temperature properties caused by the anatase–rutile phase transition has been demonstrated. It has been shown that the luminescence of rutile films is longer, for both TiO_2 nanoparticles and nanotubes. Photovoltaic cells of the DSSC type have been assembled on the basis of the obtained nanostructures. Impedance spectroscopy has demonstrated that the resistance to electron transport in films of TiO_2 nanotubes is higher and the recombination rate is lower than in films of nanoparticles.

Keywords: nanoparticle, nanotube, titanium dioxide, luminescence, dye-sensitized solar cell, photovoltaics, luminescence spectroscopy

DOI: 10.1134/S0036023621010071

Titanium dioxide (TiO_2) belongs to the class of wide-gap semiconductors widely used in photocatalysis, medicine, ecology, and dye-sensitized solar cells (DSSC) [1–4]. In DSSCs, TiO_2 is a matrix onto which dye molecules are adsorbed. Therefore, the larger its specific surface area, the higher the cell efficiency [5, 6]. An important role for the operation of photocells is played by the rate of electron transport through the oxide semiconductor to the current collector. Using various synthetic approaches, it is possible to obtain nanostructures in the form of nanoparticles (NPs) [7, 8], nanotubes (NTs) [9], nanorods [10], and nanowires [11]. The structures most frequently used in DSSCs are TiO_2 NPs. For example, in films made of TiO_2 NPs, three-dimensional electron transport can occur, and the contacts between them, formed during heat treatment, affect the possibility of electron transfer from one NP to another. Contacts that have not formed due to uneven heating of the sample lead to a decrease in the efficiency of this process. One-dimensional nanostructures, such as NTs, can have a number of advantages over NPs. In this case, the electron transport is possible only in one direction, namely, along the walls. This can lead to a decrease in the travel time of electrons from the centers of charge generation to the collector electrodes. Due to the more regular structure of NTs, it is possible to significantly reduce the number of surface defects that impede the electron transport [12]. The presence of defects in nanostructures can create additional electronic levels localized in the band gap of a semiconductor, which affect its optical and electrical properties and, consequently, the efficiency of solar energy conversion into electrical energy [13–15]. One of the efficient and sensitive methods for assessing the defect content of the TiO_2 structure is photoluminescence spectroscopy [16–19]. It should be noted that most studies are associated with titanium dioxide NPs with an anatase or rutile structure [20]. The luminescent properties of TiO_2 NTs obtained by electrochemical anodization and the effect of the dioxide structure on their photovoltaic properties have been insufficiently studied [21]; therefore, their detailed study is the purpose of this work.

EXPERIMENTAL

Fabrication of Films of TiO_2 NPs

To prepare a TiO_2 NP film on the surface of FTO supports (fluorine-doped tin oxide) (8 Ω/cm^2, Sigma Aldrich), commercially available Degussa P-25 powder (Sigma Aldrich) was used. In the course of synthesis, the powder was triturated in a porcelain mortar with small amounts of deionized water and acetone taken in the 10 : 1 ratio (v/v). For optical measurements, this paste was applied to the surface of nonluminescing quartz; for DSSC assembling, the paste was applied to glasses with an FTO conducting layer by the doctor blade method, depending on the studies

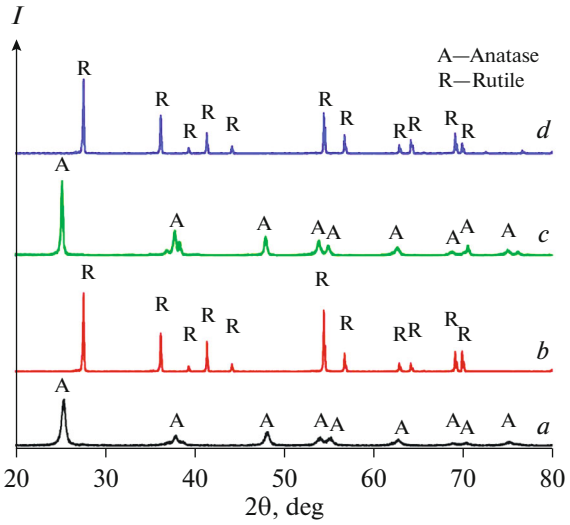

Fig. 1. X-ray powder diffraction patterns of TiO_2 samples: (a) TiO_2 NPs (773 K), (b) TiO_2 NPs (1273 K), (c) TiO_2 NTs (773 K), and (d) TiO_2 NTs (1273 K).

performed. The resulting films were annealed in an SNOL high-temperature furnace (PL 20/12.5, Russia) at 773 and 1273 K for 2 h.

Synthesis of TiO_2 NTs

TiO_2 NTs were synthesized by three-stage electrochemical anodizing of a titanium foil (VT1-0, 99.7%) preliminarily subjected to chemical polishing. $C_2H_6O_2$ containing 0.5 wt % NH_4F and 3 wt % H_2O was used as an electrolyte. The anodic oxidation temperature was 5–7°C. Platinum foil served as the cathode. The anodizing voltage was 50 V. The film obtained at the first stage of anodizing during 2 h was removed from the titanium foil in an ultrasonic bath in a 1 M hydrochloric acid solution to exclude hydrolysis products on the NT surface. The second stage lasted 24 h, during which an array of nanotubes was formed. At the third stage of anodization, the films formed by titania NTs were separated from the titanium foil [22]. Then, the resulting films were annealed at 773 and 1273 K for 2 h.

SEM images of the surface of the samples were obtained on a Tescan MIRA 3LMU scanning electron microscope. The voltage on the accelerating electrode was 20 keV. The morphology was studied in secondary electron mode.

The phase composition of the samples was determined using X-ray diffraction patterns obtained on a STOE STADI-P automatic powder diffractometer (CuK_α radiation, λ = 1.54056 Å). The diffraction patterns were recorded in the 2θ range of 5°–80° with a 5-s exposure and a 0.02° step. X-ray diffraction patterns were analyzed using the PDF-2 powder database and the standard WinXPow software package. The spectral and kinetic characteristics of the films were determined on an automated setup operating in the photon counting mode at the temperature of liquid nitrogen. Excitation was carried out with an AIL-3 nitrogen laser (λ_{gen} = 337 nm, E = 30 μJ, τ_p = 10 ns). Before measurements, the sample was placed in an optical cryostat, which was preliminarily evacuated to a residual pressure of $p = 5 \times 10-4$ mbar.

DSSC Assembling

The DSSC was assembled according to the procedure described in [23]. Films formed by titania NPs and NTs were immersed in an alcohol solution of N719 ruthenium dye (di-tetrabutylammonium *cis*-bis(isothiocyanato)bis(2,2'-bipyridyl-4,4'-dicarboxylato)ruthenium(II), Sigma Aldrich) for 24 h. Platinum counter electrodes were electrochemically deposited from H_2PtCl_6. The electrodes were sealed using a Solaronix Meltonix sealant. Solaronix iodolyte H30 was used as the electrolyte. The current–voltage characteristics and cell efficiency were determined on a Pet CT50AAA cell tester with a light power of 100 mW/cm^2 (Air Mass 1.5). Electrochemical impedance spectra were recorded on an Elins Z-500PRO setup (Russia). The amplitude of the applied signal was 20 mV, the frequency was varied from 1 MHz to 100 mHz.

RESULTS AND DISCUSSION

Figure 1 shows the X-ray powder diffraction patterns of TiO_2 NP and NT films heat treated at 773 and 1273 K.

Strong diffraction peaks appearing at 25.28°, 37.81°, 47.99°, 53.95°, 55°, 62.9°, 68.7°, 70.3°, and 75° are indexed with Miller indices (101), (004), (200), (105), (211), (204), (116), (220) and (215), respectively, which corresponds to the anatase modification (JCPDS, no. 21-1272, anatase).

For TiO_2 NP and NT films heat treated at 1273 K, the major reflections refer to the tetragonal modification of rutile (27.4°, 36.1°, 41.3°, 54.4°, 56.53°, 62.9°, and 69.9°) and are indexed with Miller indices (110), (101), (200), (111), (210), (211), (002), (310) and (301), respectively (JCPDS, no. 21-1276, rutile).

The surface morphology of the titania NP and NT films heat treated at 773 and 1273 K, is shown in Fig. 2. Figures 2a and 2b demonstrate that the TiO_2 NP films have a pronounced granular structure. At the same magnification, it is noticeable that the film annealed at 1273 K consists of larger particles than the film annealed at 773 K. This, apparently, can be due to the fact that, under the influence of high temperature, some of the particles are sintered together, forming larger agglomerates. Figure 2c shows an SEM image of a film formed by TiO_2 NTs. It can be seen that NTs are tightly packed, and their ends are open. An increase in the annealing temperature to 1273 K also leads to a significant change in the structure (Fig. 2d): although the

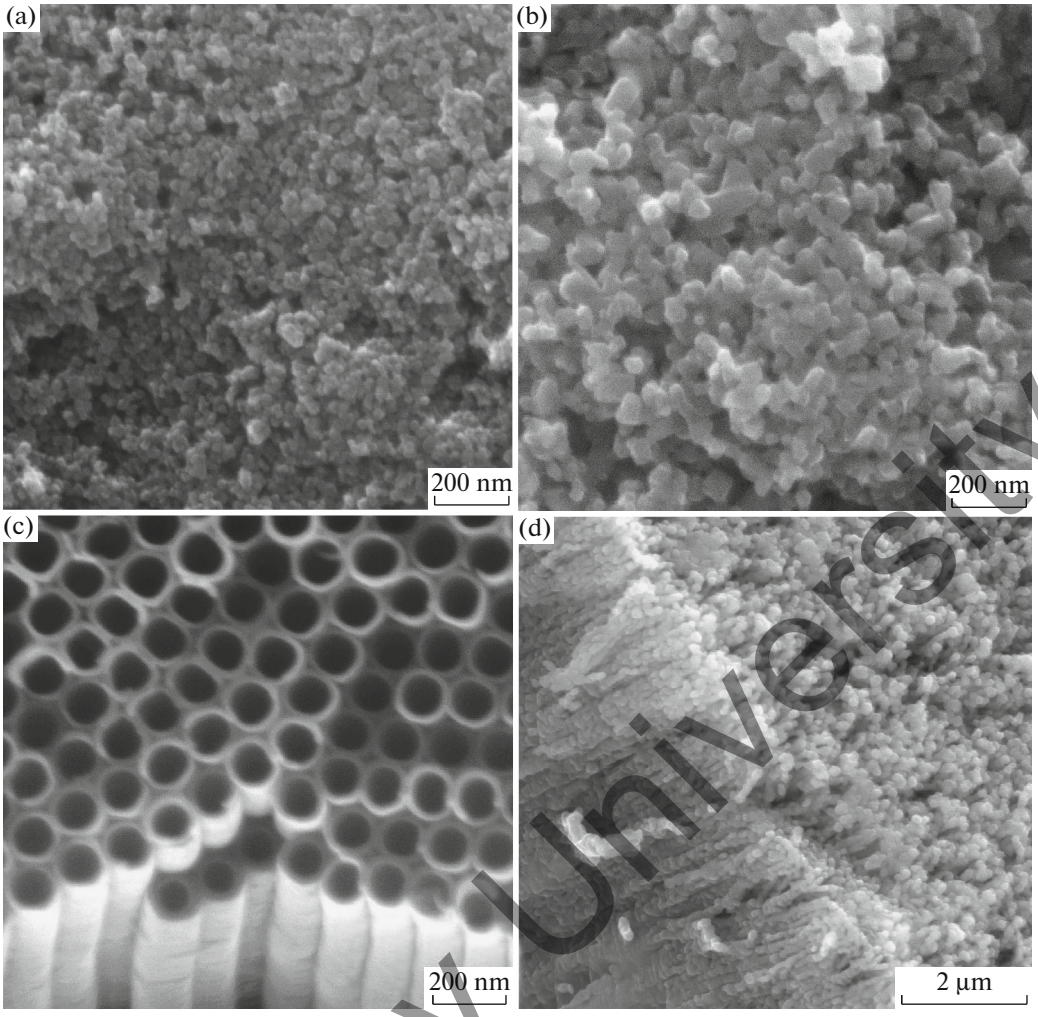

Fig. 2. SEM images of (a) TiO_2 NPs (773 K), (b) TiO_2 NPs (1273 K), (c) TiO_2 NTs (773 K), and (d) TiO_2 NTs (1273 K).

film retains its tubular structure, no open channels are observed on the surface. Analyzing the absorption spectra of TiO_2 nanostructures (Fig. 3), one can estimate their band gap using the Kubelka–Munk transformation in accordance with the formula:

$$F(R) = \frac{(1-R)^2}{2R}. \quad (1)$$

where R is the measured diffuse reflectance coefficient. The band gap was determined as the point of intersection of linear sections of the plot of $\sqrt{F(h\nu)^2} \times 10$ versus the photon energy $h\nu$. In particular, for TiO_2 NPs and NTs annealed at 773 K, the band gap was 3.20 and 3.22 eV, respectively.

For the films heat treated at 1273 K, the band gap was 3.02 eV for NPs and 3.01 eV for NTs.

The luminescence spectra and kinetics for TiO_2 NPs and NTs annealed at 773 K are shown in Figs. 4a and 4b.

No luminescence is observed for both samples at room temperature. When the films are cooled to 90 K, a broad luminescence band is observed in the wavelength range 400–700 nm, with maxima at 510 and 540 nm for TiO_2 NPs and NTs, respectively. Comparison of the luminescence spectra shows that the luminescence intensity of NTs in the 600–700 nm range is higher than that of NPs. Using approximation by Gaussian functions, deconvolution of the luminescence spectra can be performed, which is shown in Fig. 5.

The results of the approximation show that the recorded luminescence spectra are formed by three bands with maxima at 510, 540, and 600 nm. In this case, the intensity and area of the bands for NPs and NTs are different (Table 1).

The data obtained indicate that titania NPs and NTs are characterized by three luminescence centers located at different depths in the band gap; the structure of the energy levels of defects for NPs and NTs is identical, but their concentration is different. For all

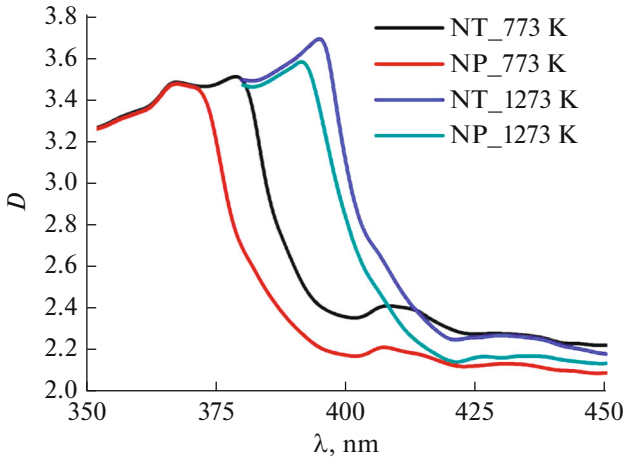

Fig. 3. Absorption spectra of nanostructured TiO_2 films.

observed luminescence centers, the luminescence decay kinetics was measured. Figure 3b shows these data for NPs and NTs measured at a wavelength of 540 nm. Kinetic curves are generally non-exponential. The lifetimes of the excited states calculated from the exponential part of the decay curves are given in Table 2.

The lifetimes of excited states of luminescence centers are different for both NPs and NTs; their values are significantly lower in the case of TiO_2 NTs. Figure 5 shows the luminescence spectra and luminescence decay kinetics of NP and NT films annealed at 1273 K. For both samples, a luminescence spectrum characteristic of the rutile modification is observed, with a maximum at 850 nm (Fig. 6a). It should be noted that the luminescence intensity for NPs is much higher than for NTs.

Figure 6b also shows the luminescence decay kinetics of NPs and NTs. The excitation wavelength was 850 nm. The lifetimes of excited states were 7.5 and 8.0 ms for NPs and NTs, respectively.

On the basis of the obtained films, DSSCs have been assembled, and their current–voltage characteristics have been measured (Fig. 7).

Based on the obtained curves, the key parameters of the assembled solar cells have been determined (Table 3).

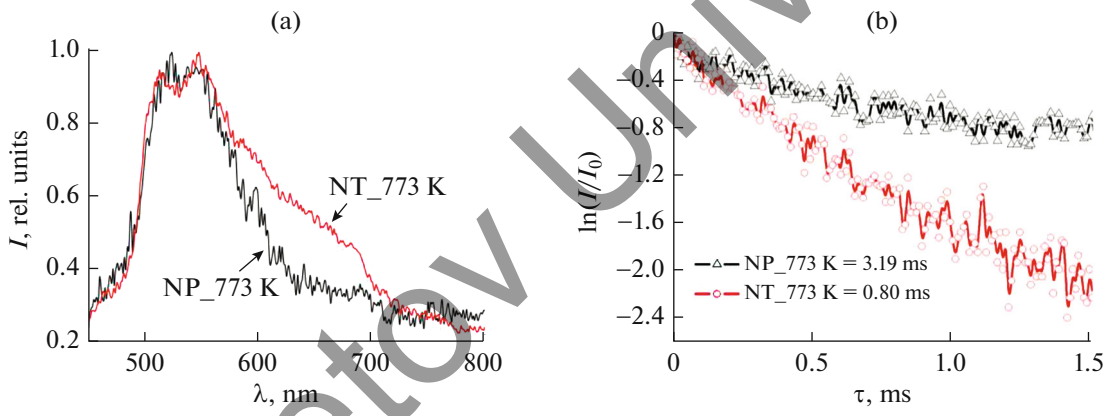

Fig. 4. (a) Normalized luminescence spectra and (b) luminescence duration kinetics of TiO_2 NPs and NTs.

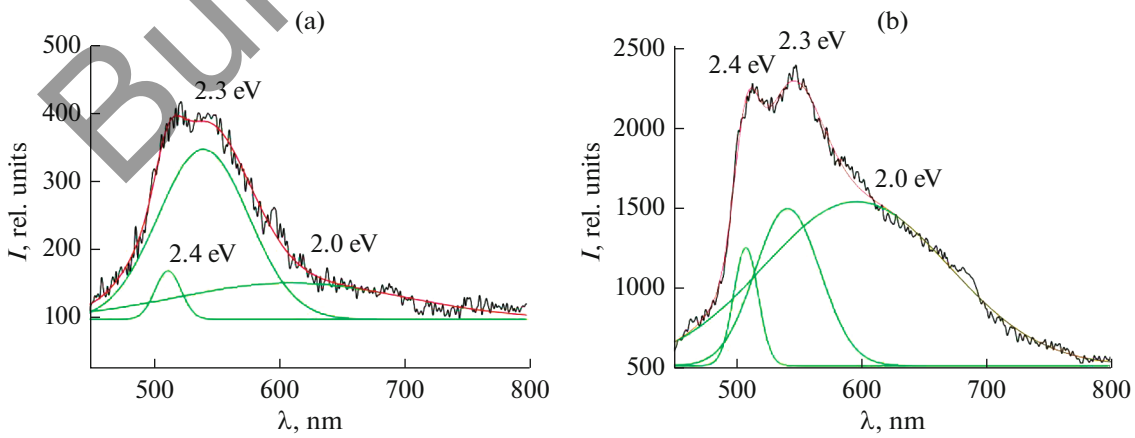

Fig. 5. Deconvolution of luminescence spectra of (a) TiO_2 NPs and (b) TiO_2 NTs annealed at 773 and 90 K.

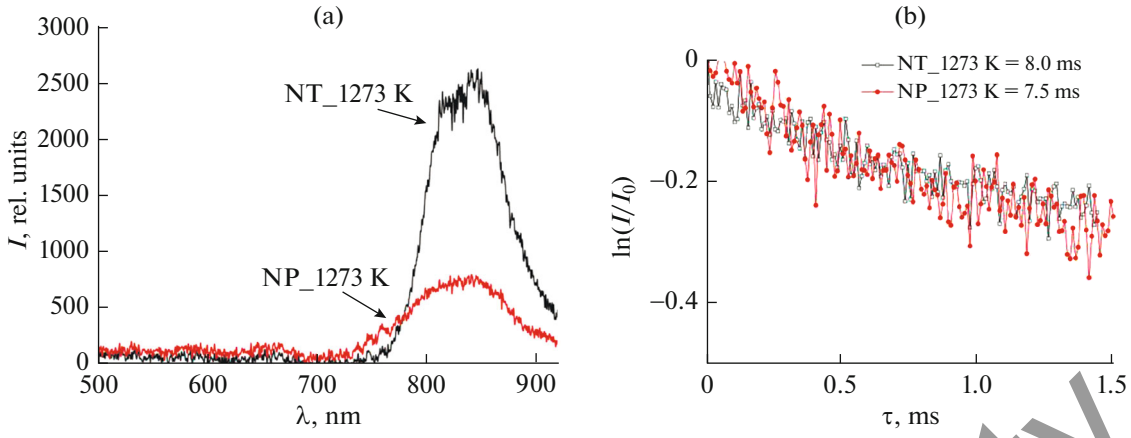

Fig. 6. Spectral and kinetic properties of TiO_2 films annealed at 1273 K.

It can be seen from the presented data that the characteristics of cells based on anatase NP and NT films are higher than those for films of a rutile structure, which is in good agreement with the data presented in the literature for other types of TiO_2 nanostructures. For cells based on anatase, the voltage is slightly higher than for assemblies based on rutile. As a rule, the voltage in such solar cells is determined by the position of the quasi-Fermi level. From the impedance spectra (Fig. 8), the key electrical transport properties of TiO_2 films were calculated; the results are given in Table 4.

From the presented data, it can be seen that the impedance spectrum consists of several circles. Using the technique described in [24, 25], from the central arc of the impedance spectra, we calculated the effective electron diffusion coefficient D_{eff}, the effective recombination rate k_{eff}, the effective electron lifetime τ_{eff}, the resistance to electron transport in the titania film R_w, and the charge transfer resistance R_k related to electron recombination.

Data in Table 4 indicate that the resistance to electron transport in TiO_2 (R_w) for NT films is higher than for NP films. In this case, the recombination rate (k_{eff}) in NT-based films is lower than k_{eff} of the cells based on NPs of the same TiO_2 modification. This is probably due to the technology of manufacturing NT-based DSSCs. A paste based on TiO_2 NPs and an aqueous solution of $TiCl_4$ (30 mmol/L) is used for grafting an NT-based film to a substrate with a conductive FTO coating. An additional resistance to electron transport in the cell arises at the NT–NP interface. The recombination resistance value (Table 4) indicates a high recombination rate observed in cells based on rutile NTs and NPs; this is supported by the low effective lifetime of an electron for cells based on NTs and NPs. The R_k value is also significantly influenced by the specific surface area of the material. With the same phase of the materials used for manufacturing DSSCs (anatase or rutile), the R_k value is higher for films with a high specific surface area. On the basis of the formula $k_{eff} = 2N_s k_r$ (N_s is the electron density at defect energy levels (cm^{-3}), k_r is the recombination rate constant (cm^3/s) of electrons from TiO_2 defect levels into the electrolyte [25]), it can be concluded that the concentration of defects through which recombination processes occur in rutile NP and NT films is higher than in anatase.

Table 1. Intensities and areas of bands obtained by Gauss approximation of luminescence spectra of TiO_2 NP and NT films

Parameter	NP	NT
	510 nm	
S, %	5.2	6.7
I, rel. units	65	736
	540 nm	
S, %	72.7	23.5
I, rel. units	250	980
	600 nm	
S, %	22.1	69.8
I, rel. units	46	1023

Table 2. Luminescence duration of TiO_2 NP and NT films at different wavelengths at 773 K

Sample	Luminescence duration of films, ns		
	luminescence wavelength, nm		
	510	540	600
NP	6.2	3.0	6.7
NT	2.5	0.8	6.3

Table 3. Key parameters of DSSCs

Sample	Voltage, V	Photocurrent, A/cm^2	Filling factor	Efficiency, %
NP_773 K	0.69	0.014	0.62	4.10
NP_1273 K	0.68	0.003	0.60	1.32
NT_773 K	0.65	0.010	0.56	3.80
NT_1273 K	0.60	0.005	0.38	1.36

Table 4. Electrical transport parameters of solar cells

Sample	D_{eff}, cm^2/s	k_{eff}, s^{-1}	τ_{eff}, s	R_k, Ω	R_w, Ω
TiO_2 NP_773 K	9.9×10^{-5}	14.0	0.07	22.0	*26*
TiO_2 NP_1273 K	4.7×10^{-5}	57.0	0.02	175.0	*26*
TiO_2 NT_773 K	5.5×10^{-5}	3.6	0.27	17.5	36
TiO_2 NT_1273 K	2.9×10^{-5}	25.3	0.04	38.0	40

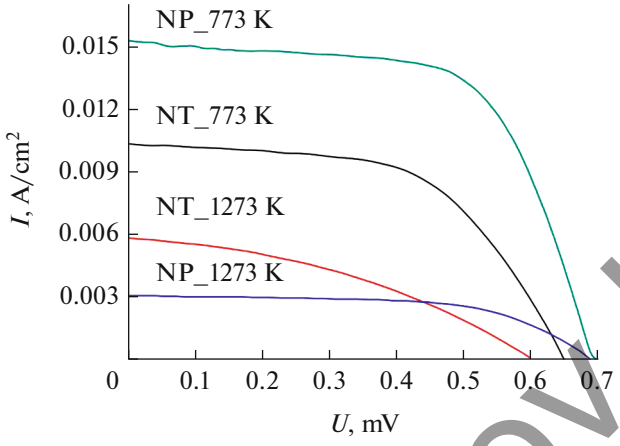

Fig. 7. Current–voltage characteristics of solar cells based on TiO_2 films.

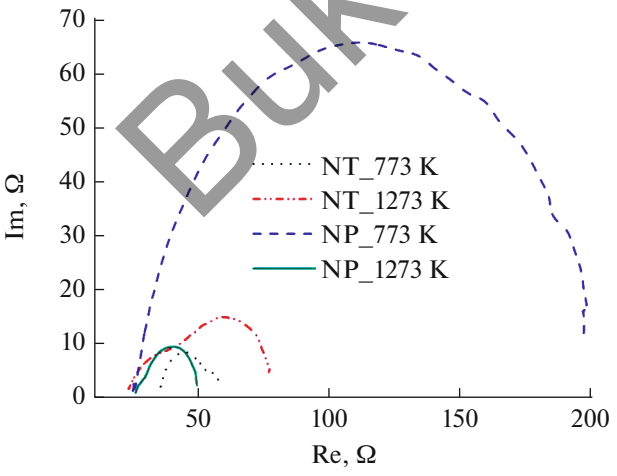

Fig. 8. Impedance spectra of solar cells.

CONCLUSIONS

Nanocrystalline titania films consisting of TiO_2 NPs and NTs have been fabricated; their photoluminescent properties have been studied at 90 K. The effect of heat treatment on spectral properties due to a change in the structure type from anatase to rutile has been demonstrated. It has been shown that the luminescence of anatase NP and NT films occurs from defect levels of different energies. In the anatase modification, the luminescence duration of NP films was 3 ms, and that from NT films was 0.8 ms. It has been found that the luminescence of rutile films is longer, both for TiO_2 NPs and NTs. When assembling DSSCs, cells based on anatase films had a higher efficiency than cells with rutile films. It has been found that the recombination rate in films based on NTs is lower, but the resistance to electron transport is higher than in films based on NPs. It has been shown that the concentration of defects through which the recombination processes occur in rutile NP and NT films is higher than in anatase.

FUNDING

The work was carried out within the framework of grants from the Committee for Science of the Ministry of Education and Science of the Republic of Kazakhstan (program type A, nos. APP-PHD-A-19/004P and AP08052675: grants for supporting studies and trainings of PhDs), as well as State Assignment of Kurnakov Institute of General and Inorganic Chemistry, RAS in the field of basic research and State budget topic of the Chemistry Department of Moscow State University “Catalysis and Physical Chemistry of Surfaces” (no. AAAA-A16-116092810057-8).

CONFLICT OF INTEREST

The authors declare no conflict of interest.

REFERENCES

1. A. Fujishima and K. Honda, Nature **238**, 37 (1972). https://doi.org/10.1038/238037a0
2. T. M. Serikov, N. K. Ibrayev, N. Nuraje, et al., Russ. Chem. Bull. **66**, 614 (2017). https://doi.org/10.1007/s11172-017-1781-0
3. S. Ito, T. N. Murakami, P. Comte, et al., Thin Solid Films **516**, 4613 (2008). https://doi.org/10.1016/j.tsf.2007.05.090
4. J. Lee, K. S. Hong, K. Shin, et al., J. Ind. Eng. Chem. **18**, 19, (2012). https://doi.org/10.1016/j.jiec.2011.11.116
5. C. Yang, H. Fan, Y. Xi, et al., Appl. Surf. Sci. **254**, 2685 (2008). https://doi.org/10.1016/j.apsusc.2007.10.006
6. Z. A. Fattakhova, G. S. Zakharova, E. I. Andreikov, et al., Russ. J. Inorg. Chem. **64**, 857 (2019). https://doi.org/10.1134/S0036023619070076
7. J. Yang, S. Mei, and J. Ferreira, Mater. Sci. Eng. C **15**, 183 (2001). https://doi.org/10.1016/S0928-4931(01)00274-0
8. D. A. Zherebtsov, S. A. Kulikovskikh, V. V. Viktorov, et al., Russ. J. Inorg. Chem. **64**, 165 (2019). https://doi.org/10.1134/S0036023619020220
9. X. Wu, Q. Z. Jiang, Z. F. Ma, et al., Solid State Commun. **136**, 513 (2005). https://doi.org/10.1016/j.ssc.2005.09.023
10. K. Fujihara, A. Kumar, R. Jose, et al., Nanotechnology **18**, 36709 (2007). https://doi.org/10.1088/0957-4484/18/36/365709
11. E. Arcadipane, R. Sanz, M. Miritello, et al., Mater. Sci. Semicond. Process. **42**, 24 (2016). https://doi.org/10.1016/j.mssp.2015.07.055
12. D. Mukul and H. Hongshan, Rijeka: InTech **27**, 537 (2012). https://doi.org/10.5772/36332
13. S. D. Mo and W. Y. Ching, Phys. Rev. B **51**, 13024 (1995). https://doi.org/10.1103/PhysRevB.51.13023
14. O. Carp, C. L. Huisman, and A. Reller, Prog. Solid State Chem. **32**, 33 (2004). https://doi.org/10.1016/j.progsolidstchem.2004.08.001
15. M. Landmann, E. Rauls, and W. G. Schmidt, J. Phys.: Condens. Matter **24**, 195503 (2012). https://doi.org/10.1088/0953-8984/24/19/195503
16. V. M. Ievlev, S. Kushev, and A. N. Latyshev, et al., Condens. Matter Interphases **2**, 141 (2012).
17. X. Wang, Z. Feng, J. Shi, and G. Jia, Phys. Chem. Chem. Phys. **12**, 7083 (2010). https://doi.org/10.1039/B925277K
18. H. Nakajima, T. Mori, and M. Watanabe, J. Appl. Phys. **96**, 925 (2004). https://doi.org/10.1063/1.1757649
19. N. Serpone, D. Lawless, and R. Khairutdinov, J. Phys. Chem. **99**, 16646 (1995). https://doi.org/10.1021/j100045a026
20. C. Mercado, Z. Seeley, A. Bandyopadhyay, et al., ACS Appl. Mater. Interfaces **3**, 2281 (2011). https://doi.org/10.1021/am2006433
21. R. R. Sanjines, H. Tang, H. Berger, et al., J. Appl. Phys. **75**, 2945 (1994). https://doi.org/10.1063/1.356190
22. J. Lin, J. Chen, and X. Chen, Electrochem. Commun. **12**, 1062 (2010). https://doi.org/10.1016/j.elecom.2010.05.027
23. U. Bach, D. Lupo, P. Comte, et al., Nature **395**, 583 (1998). https://doi.org/10.1038/26936
24. F. Fabregat-Santiago, J. Bisquert, G. Garcia-Belmonte, et al., Sol. Energy Mater. Sol. Cells **87**, 117 (2019). https://doi.org/10.1016/j.solmat.2004.07.017
25. M. Adachi, M. Sakamoto, J. Jiu, et al., J. Phys. Chem. B **110**, 13872 (2006). https://doi.org/10.1021/jp061693u

Translated by G. Kirakosyan